Appendix A

Observation History

The following tables contain the details of every observation used to generate the 10 constituent survey maps. Gaps in the run of observation number indicate observations that were discarded because of technical or data quality problems. The right ascension and declination limits of the final maps are listed at the top of each table.

Map 1 / A12D63			Start RA	End RA	Low Dec	High Dec
			12h00m00s	22h00m00s	−63°	−24°
Obs	Date	Raster				
19	162/1980	0	10h20m48s	0h16m00s	−63°	−24°
20	163/1980	4	9h56m48s	0h04m48s	−63°	−24°
21	165/1980	2	10h02m24s	0h04m00s	−63°	−24°
22	166/1980	6	9h51m12s	0h05m36s	−63°	−24°
23	167/1980	1	9h55m36s	23h38m00s	−63°	−24°
24	168/1980	5	9h06m00s	23h14m00s	−63°	−24°
25	169/1980	3	8h58m48s	23h19m36s	−63°	−24°
26	171/1980	7	9h00m24s	23h14m48s	−63°	−24°
27	172/1980	0	10h01m36s	0h03m12s	−63°	−24°
34	189/1980	1	9h55m36s	23h38m00s	−63°	−24°
35	190/1980	2	15h48m00s	23h12m48s	−63°	−24°
36	191/1980	3	8h58m48s	22h47m36s	−63°	−24°
37	194/1980	4	11h00m48s	0h24m00s	−63°	−24°
38	195/1980	5	11h01m12s	0h24m00s	−63°	−24°
39	196/1980	6	11h01m36s	1h03m12s	−63°	−24°
40	197/1980	7	10h55m36s	1h16m24s	−63°	−24°
41	202/1980	0	11h56m48s	1h26m24s	−63°	−24°
42	203/1980	2	11h00m00s	1h14m24s	−63°	−24°
43	204/1980	1	11h57m12s	1h52m24s	−63°	−24°
44	205/1980	3	12h30m00s	1h53m12s	−63°	−24°
45	206/1980	6	11h59m12s	1h35m12s	−63°	−24°
46	207/1980	4	11h58m24s	2h00m00s	−63°	−24°
47	208/1980	7	12h02m48s	2h52m24s	−63°	−24°
48	209/1980	5	11h58m48s	1h54m00s	−63°	−24°

Map 2 / A23D80			Start RA	End RA	Low Dec	High Dec
			23h00m00s	7h00m00s	−80°	−61°
Obs	Date	Raster				
182	266/1982	2	19h56m48s	7h49m36s	−80°	−61°
183	269/1982	0	20h00m00s	7h48m00s	−80°	−61°
184	275/1982	1	20h00m48s	8h22m24s	−80°	−61°
185	276/1982	2	19h56m48s	8h04m00s	−80°	−61°
186	280/1982	0	20h00m00s	8h02m24s	−80°	−61°
187	288/1982	1	20h00m48s	8h17m36s	−80°	−61°
188	310/1982	2	19h56m48s	7h20m48s	−80°	−61°
189	311/1982	0	20h00m00s	7h19m12s	−80°	−61°
190	338/1982	1	20h00m48s	6h56m00s	−80°	−61°

Map 3 / A05D63			Start RA	End RA	Low Dec	High Dec
			5h00m00s	13h20m00s	−63°	−24°
Obs	Date	Raster				
199	85/1986	0	5h00m48s	17h20m00s	−63°	−24°
200	86/1986	1	5h01m12s	17h20m24s	−63°	−24°
201	88/1986	2	4h29m36s	17h20m48s	−63°	−24°
202	89/1986	3	4h55m36s	17h21m12s	−63°	−24°
203	90/1986	4	4h56m00s	17h21m36s	−63°	−24°
204	98/1986	5	4h56m24s	17h34m48s	−63°	−24°
205	100/1986	6	4h56m48s	17h35m12s	−63°	−24°
206	112/1986	7	4h57m12s	17h54m48s	−63°	−24°
207	113/1986	0	5h00m48s	17h58m24s	−63°	−24°
208	114/1986	1	5h01m12s	17h58m48s	−63°	−24°
209	116/1986	2	5h01m36s	18h05m36s	−63°	−24°
210	117/1986	3	4h55m36s	17h59m36s	−63°	−24°
211	116/1986	4	4h30m24s	18h06m24s	−63°	−24°
212	121/1986	5	4h30m48s	18h13m12s	−63°	−24°
213	122/1986	6	4h56m48s	18h13m36s	−63°	−24°
214	123/1986	7	4h57m12s	18h14m00s	−63°	−24°
215	127/1986	1	5h01m12s	18h24m24s	−63°	−24°
216	128/1986	4	4h56m00s	18h25m36s	−63°	−24°
217	130/1986	4	4h56m00s	18h25m36s	−63°	−24°
218	131/1986	5	4h56m24s	14h00m24s	−63°	−24°
219	133/1986	3	4h55m36s	18h31m36s	−63°	−24°
220	135/1986	0	5h00m48s	18h43m12s	−63°	−24°
221	137/1986	0	5h00m48s	18h43m12s	−63°	−24°

Map 4 / A14D26			Start RA	End RA	Low Dec	High Dec
			14h00m00s	2h30m00s	−26°	+13°
Obs	Date	Raster				
222	182/1986	0	13h58m24s	3h28m00s	−26°	+13°
223	186/1986	1	13h50m48s	2h50m00s	−26°	+13°
224	184/1986	2	13h59m12s	3h09m36s	−26°	+13°
225	191/1986	3	13h59m36s	4h14m00s	−26°	+13°
226	183/1986	4	14h00m00s	3h23m12s	−26°	+13°
227	187/1986	5	14h00m24s	2h51m36s	−26°	+13°
228	185/1986	6	14h00m48s	3h11m12s	−26°	+13°
229	214/1986	7	14h01m12s	3h30m48s	−26°	+13°
230	215/1986	0	13h58m24s	3h28m00s	−26°	+13°
231	194/1986	4	14h00m00s	4h14m24s	−26°	+13°
232	216/1986	2	13h59m12s	3h28m48s	−26°	+13°
233	219/1986	6	14h00m48s	3h24m00s	−26°	+13°
234	220/1986	1	13h58m48s	3h22m00s	−26°	+13°
235	221/1986	5	14h00m24s	3h23m36s	−26°	+13°
236	222/1986	3	13h59m36s	3h22m48s	−26°	+13°
238	227/1986	7	14h01m12s	3h16m00s	−26°	+13°

Map 5 / A06D83			Start RA	End RA	Low Dec	High Dec
			6h00m00s	18h00m00s	−83°	−61°
Obs	Date	Raster				
240	111/1987	0	6h00m00s	19h00m00s	−83°	−61°
241	113/1987	1	6h48m00s	19h10m42s	−83°	−61°
242	122/1987	2	5h56m48s	18h47m12s	−83°	−61°
243	120/1987	0	6h00m00s	18h43m48s	−83°	−61°
244	123/1987	1	6h00m48s	18h56m00s	−83°	−61°
245	116/1987	2	6h30m24s	18h28m00s	−83°	−61°
246	133/1987	0	6h00m00s	19h33m36s	−83°	−61°
247	134/1987	1	6h00m48s	19h39m12s	−83°	−61°
248	124/1987	2	5h56m48s	18h52m00s	−83°	−61°

Map 6 / A12D11			Start RA	End RA	Low Dec	High Dec
			12h00m00s	24h00m00s	+11°	+32°
Obs	Date	Raster				
250	138/1987	0	11h00m00s	0h50m00s	+11°	+32°
253	172/1987	3	10h57m12s	1h39m12s	+11°	+32°
254	176/1987	4	10h57m36s	1h43m36s	+11°	+32°
255	180/1987	0	11h00m00s	17h52m00s	+11°	+32°
256	183/1987	1	11h00m24s	1h46m24s	+11°	+32°
257	189/1987	2	11h00m48s	0h10m48s	+11°	+32°
258	196/1987	3	10h57m12s	1h31m12s	+11°	+32°
259	197/1987	4	10h57m36s	1h07m36s	+11°	+32°
260	204/1987	1	11h00m24s	1h26m24s	+11°	+32°
261	211/1987	2	11h00m48s	1h14m48s	+11°	+32°
262	222/1987	0	11h00m00s	1h02m00s	+11°	+32°

Map 7 / A14D83			Start RA	End RA	Low Dec	High Dec
			14h00m00s	1h00m00s	−83°	−61°
Obs	Date	Raster				
291	177/1989	0	14h00m00s	3h33m36s	−83°	−61°
292	178/1989	1	14h00m48s	3h15m12s	−83°	−61°
293	180/1989	2	13h56m48s	3h30m24s	−83°	−61°
294	181/1989	0	14h00m00s	3h09m36s	−83°	−61°
295	182/1989	1	13h56m00s	3h39m12s	−83°	−61°
296	183/1989	2	13h56m48s	3h11m12s	−83°	−61°
297	185/1989	0	14h00m00s	2h26m24s	−83°	−61°
298	193/1989	1	13h56m00s	4h03m12s	−83°	−61°
299	199/1989	2	13h56m48s	3h49m36s	−83°	−61°

Map 8 / A22D26			Start RA	End RA	Low Dec	High Dec
			22h00m00s	7h00m00s	−26°	+13°
Obs	Date	Raster				
311	276/1990	0	21h58m24s	10h43m12s	−26°	+13°
312	277/1990	1	21h58m48s	9h39m36s	−26°	+13°
313	278/1990	2	21h59m12s	10h56m48s	−26°	+13°
314	282/1990	3	19h58m00s	10h57m12s	−26°	+13°
315	290/1990	4	22h00m00s	11h29m36s	−26°	+13°
316	319/1990	5	21h54m00s	10h26m00s	−26°	+13°
317	320/1990	6	21h54m24s	9h03m12s	−26°	+13°
318	323/1990	7	21h54m28s	10h33m12s	−26°	+13°
319	332/1990	0	21h58m24s	10h43m12s	−26°	+13°
320	333/1990	1	21h58m48s	9h14m00s	−26°	+13°
321	343/1990	2	23h54m24s	9h56m00s	−26°	+13°
322	351/1990	3	22h57m12s	11h42m00s	−26°	+13°
323	352/1990	4	22h57m36s	11h29m36s	−26°	+13°
324	361/1990	5	22h58m00s	10h45m12s	−26°	+13°
325	11/1991	6	22h58m24s	12h02m24s	−26°	+13°
326	15/1991	7	23h56m24s	11h05m12s	−26°	+13°

Map 9 / A04D26			Start RA	End RA	Low Dec	High Dec
			4h00m00s	15h00m00s	−26°	+13°
Obs	Date	Raster				
450	66/1992	0	3h56m48s	15h56m48s	−26°	+13°
451	67/1992	1	1h55m36s	15h31m36s	−26°	+13°
452	68/1992	2	3h57m56s	15h25m36s	−26°	+13°
453	72/1992	3	2h54m00s	15h38m48s	−26°	+13°
454	73/1992	4	3h13m36s	15h32m48s	−26°	+13°
455	74/1992	5	21h54m00s	15h39m36s	−26°	+13°
456	76/1992	6	2h29m36s	15h40m00s	−26°	+13°
457	77/1992	7	1h58m00s	15h59m36s	−26°	+13°
458	81/1992	0	3h56m48s	16h03m12s	−26°	+13°
459	82/1992	1	3h25m12s	16h10m00s	−26°	+13°
462	91/1992	4	3h58m24s	16h30m24s	−26°	+13°
463	93/1992	5	3h58m48s	16h24m24s	−26°	+13°
464	96/1992	6	3h59m12s	16h37m36s	−26°	+13°
465	97/1992	7	3h59m36s	15h38m00s	−26°	+13°
466	98/1992	2	3h57m36s	16h36m00s	−26°	+13°
467	112/1992	3	3h58m00s	17h59m36s	−26°	+13°

Map 10 / A21D63			Start RA	End RA	Low Dec	High Dec
			21h00m00s	7h00m00s	−63°	−24°
Obs	Date	Raster				
330	284/1991	0	19h56m48s	8h16m00s	−63°	−24°
331	290/1991	1	19h57m12s	9h07m36s	−63°	−24°
332	291/1991	2	19h57m36s	7h57m36s	−63°	−24°
333	301/1991	3	19h58m00s	7h38m48s	−63°	−24°
334	326/1991	4	20h56m00s	7h58m24s	−63°	−24°
335	327/1991	5	20h56m24s	7h58m48s	−63°	−24°
336	310/1991	6	22h26m24s	7h33m36s	−63°	−24°
337	328/1991	7	20h57m12s	7h59m36s	−63°	−24°
471	287/1992	1	19h44m24s	9h26m48s	−63°	−24°
472	289/1992	2	20h36m00s	8h55m12s	−63°	−24°
473	290/1992	3	20h55m36s	9h40m24s	−63°	−24°
474	291/1992	4	20h56m00s	9h40m48s	−63°	−24°
475	292/1992	5	20h56m24s	9h47m36s	−63°	−24°
479	348/1992	1	20h29m12s	7h47m36s	−63°	−24°
480	322/1992	2	20h23m12s	8h04m00s	−63°	−24°
481	321/1992	3	20h30m00s	8h04m24s	−63°	−24°
482	350/1992	4	20h56m00s	7h39m12s	−63°	−24°
484	320/1992	6	20h56m48s	8h05m36s	−63°	−24°
485	332/1992	7	20h06m00s	75h3m12s	−63°	−24°
486	300/1992	6	20h50m24s	9h54m24s	−63°	−24°
488	312/1992	7	20h57m12s	82h5m12s	−63°	−24°

Appendix B

Mathematical Supplement

This appendix provides supplementary mathematical background that is required for chapter 4.

B.1 Definition of Source Flux

The monochromatic flux of a radio source centred on spherical polar coordinate Ω_0 is related to its intrinsic brightness distribution by the following integral equation (Kraus, 1966f):

$$S_\lambda = 10^{26} \times \iint_{\Omega_S} B_\lambda(\Omega_0 + \Omega')\, d\Omega' = \frac{2k \times 10^{26}}{\lambda^2} \iint_{\Omega_S} T_B(\Omega_0 + \Omega')\, d\Omega' \quad [\mathrm{Jy}] \tag{B.1}$$

where the source is assumed to subtend the finite solid angle Ω_S. $T_B(\Omega)$ is the Rayleigh-Jeans brightness temperature towards direction Ω, k is Boltzmann's constant, and λ is the nominal wavelength of the observation. Note that the sum or difference of solid angles $(\Omega_0 + \Omega')$ implies an Euler coordinate rotation rather than a linear shift of origin.

B.2 Integrating P_N

At this point it is convenient to introduce a quantity that will be called the *partial beam solid angle*, which is defined thus:

$$\Omega_a(\theta_R) = \int_0^{\theta_R} \int_0^{2\pi} P_N(\Omega)\, \sin\theta\, d\theta\, d\phi = \iint_{\Omega_R} P_N(\Omega)\, d\Omega \quad [\mathrm{sr}] \tag{B.2}$$

This is the effective solid angle subtended by the beam out to a small-circle radius of θ_R [rad] or, equivalently, within a cone of solid angle given by:

$$\Omega_R = \int_0^{\theta_R} \int_0^{2\pi} d\Omega \quad [\mathrm{sr}] \tag{B.3}$$

It is obvious from the definition of the *beam solid angle* that $\Omega_a(\pi) = \Omega_A$.

B.3 Integrating T_A

Given a radio image of a source, its flux may be estimated by numerical integration of the observed excess antenna temperature brightness distribution. Beam smoothing increases

the apparent extent of the source, hence increasing the solid angle necessary for the integration. Source confusion and numerical instability impose practical limits on the extent of the flux integration. The *partial flux* that results from integrating a source image (centred on Ω_0) out to a small-circle radius of $\theta_{\rm R}$ is defined to be:

$$S_\lambda(\theta_{\rm R}) = \frac{2k \times 10^{26}}{\lambda^2} \int_0^{\theta_{\rm R}} \int_0^{2\pi} T_{\rm A}(\Omega_0 + \Omega')\, d\Omega' = \frac{2k \times 10^{26}}{\lambda^2} \iint_{\Omega_{\rm R}} T_{\rm A}(\Omega_0 + \Omega')\, d\Omega' \quad [\rm Jy] \tag{B.4}$$

Substituting the convolution integral from equation 4.4 (chapter 4) into the partial flux equation above results in:

$$S_\lambda(\theta_{\rm R}) = \frac{2k \times 10^{26} \times \eta_{\rm R} \times \eta_{\rm CAL}}{\lambda^2 \times \Omega_{\rm A}} \iint_{\Omega_{\rm R}} \left[\iint_{\Omega_{\rm S}} T_{\rm B}(\Omega)\, P_{\rm N}(\Omega_0 + \Omega' - \Omega)\, d\Omega \right] d\Omega' \quad [\rm Jy] \tag{B.5}$$

B.3.1 Integration over 4π steradians

If the outer (flux) integration in equation B.5 were carried out over the whole sphere, i.e. $\theta_{\rm R} = \pi$, then the two pairs of integrals could be separated to give:

$$S_\lambda(\pi) = \left[\frac{\eta_{\rm R} \times \eta_{\rm CAL}}{\Omega_{\rm A}} \iint_{\Omega_{\rm R}=4\pi} P_{\rm N}(\Omega_0 + \Omega')\, d\Omega' \right] \left[\frac{2k \times 10^{26}}{\lambda^2} \iint_{\Omega_{\rm S}} T_{\rm B}(\Omega)\, d\Omega \right] \quad [\rm Jy] \tag{B.6}$$

which simplifies to:

$$S_\lambda(\pi) = [\eta_{\rm R} \times \eta_{\rm CAL}] \times S_\lambda \quad [\rm Jy] \tag{B.7}$$

B.3.2 Point Sources

For a point-like source equation B.5 reduces to:

$$S_\lambda(\theta_{\rm R}) = \frac{S_\lambda \times \eta_{\rm R} \times \eta_{\rm CAL}}{\Omega_{\rm A}} \iint_{\Omega_{\rm R}} \left[\iint_{\Omega_{\rm S}} \delta(\Omega - \Omega_0)\, P_{\rm N}(\Omega_0 + \Omega' - \Omega)\, d\Omega \right] d\Omega' \quad [\rm Jy] \tag{B.8}$$

which by the application of the sifting property of the delta function becomes:

$$S_\lambda(\theta_{\rm R}) = \frac{S_\lambda \times \eta_{\rm R} \times \eta_{\rm CAL}}{\Omega_{\rm A}} \iint_{\Omega_{\rm R}} P_{\rm N}(\Omega')\, d\Omega' = [\eta_{\rm R} \times \eta_{\rm CAL}] \times \frac{\Omega_{\rm a}(\theta_{\rm R})}{\Omega_{\rm A}} \times S_\lambda \quad [\rm Jy] \tag{B.9}$$

Using the beam efficiency function defined by equation 4.11 in chapter 4 this equation simplifies to:

$$S_\lambda(\theta_{\rm R}) = \eta_\Omega(\theta_{\rm R}) \times S_\lambda \quad [\rm Jy] \tag{B.10}$$

B.3.3 Extended Sources

Swapping the order of integration in equation B.5 results in:

$$S_\lambda(\theta_{\rm R}) = \frac{2k \times 10^{26} \times \eta_{\rm R} \times \eta_{\rm CAL}}{\lambda^2 \times \Omega_{\rm A}} \iint_{\Omega_{\rm S}} \left[\iint_{\Omega_{\rm R}} P_{\rm N}(\Omega_0 + \Omega' - \Omega)\, d\Omega' \right] T_{\rm B}(\Omega)\, d\Omega \quad [\rm Jy] \tag{B.11}$$

If $\theta_{\rm R}$ is much larger than the extent of the source (not necessarily point-like) and the radius of the main lobe of the beam, then the inner integral pair may be approximated by:

$$\iint_{\Omega_{\rm R}} P_{\rm N}(\Omega_0 + \Omega' - \Omega)\, d\Omega' \;\approx\; \iint_{\Omega_{\rm R}} P_{\rm N}(\Omega')\, d\Omega' = \Omega_{\rm a}(\theta_{\rm R}) \quad [\rm sr] \tag{B.12}$$

This approximation is possible because rotating the beam pattern by a Euler angle $(\Omega_0 - \Omega)$ that is much smaller than θ_R prior to the integration has little effect on the result, providing that the stray beam is weak and quasi-isotropic. Using this approximation, the two pairs of integrals may be separated, and equation B.11 simplifies to:

$$S_\lambda(\theta_R) \approx [\eta_R \times \eta_{CAL}] \times \frac{\Omega_a(\theta_R)}{\Omega_A} \times S_\lambda = \eta_\Omega(\theta_R) \times S_\lambda \quad [\text{Jy}] \tag{B.13}$$

which matches the result for point sources.

B.4 Integration of T_{FB}

The *full-beam flux* of a source centred on Ω_0 is defined to be:

$$S_{FB,\lambda} = \frac{2k \times 10^{26}}{\lambda^2} \iint_{\Omega_R} T_{FB}(\Omega_0 + \Omega)\, d\Omega \quad [\text{Jy}] \tag{B.14}$$

where θ_R, and hence Ω_R, is chosen so that the integration extends beyond the intrinsic source size by the radius of the full-beam, θ_{FB}. Following the derivation of equations B.10 and B.13 it is obvious that:

$$S_{FB,\lambda} = \frac{\eta_\Omega(\theta_R)}{\eta_{FB}} \times S_\lambda \quad [\text{Jy}] \tag{B.15}$$

Since the beam efficiency function is very nearly constant for $\theta_R > \theta_{FB}$ this equation reduces to:

$$S_{FB,\lambda} \approx S_\lambda \quad [\text{Jy}] \tag{B.16}$$

for sources of any extent.

B.5 T_{FB} for Extended Sources

If an extended source has a constant brightness distribution over a region larger than the full-beam then the excess full-beam temperature is given by (equation 4.22):

$$T_{FB} \approx \frac{1}{\Omega_{FB}} T_B \int_0^{\theta_{FB}} \int_0^{2\pi} P_N(\Omega)\, d\Omega = T_B \quad [\text{K}] \tag{B.17}$$

because the contribution of the source to the stray-beam response is almost isotropic and does not affect the differential excess temperature measurement.

Appendix C

Colour Plates

This appendix contains colour plates that are referenced in the main body of the text. The maps in **plates C.1 to C.5** are all represented as Hammer-Aitoff projections (Greisen and Calabretta, 1997) of the galactic coordinate system with the origin (i.e. the galactic centre) towards the centre of the images. The annotation of the small-circles identifying the positions of loop structures in these maps is given in the diagram below. The lines of longitude and latitude are drawn at 30° intervals in all of the images in plates C.1 to C.5.

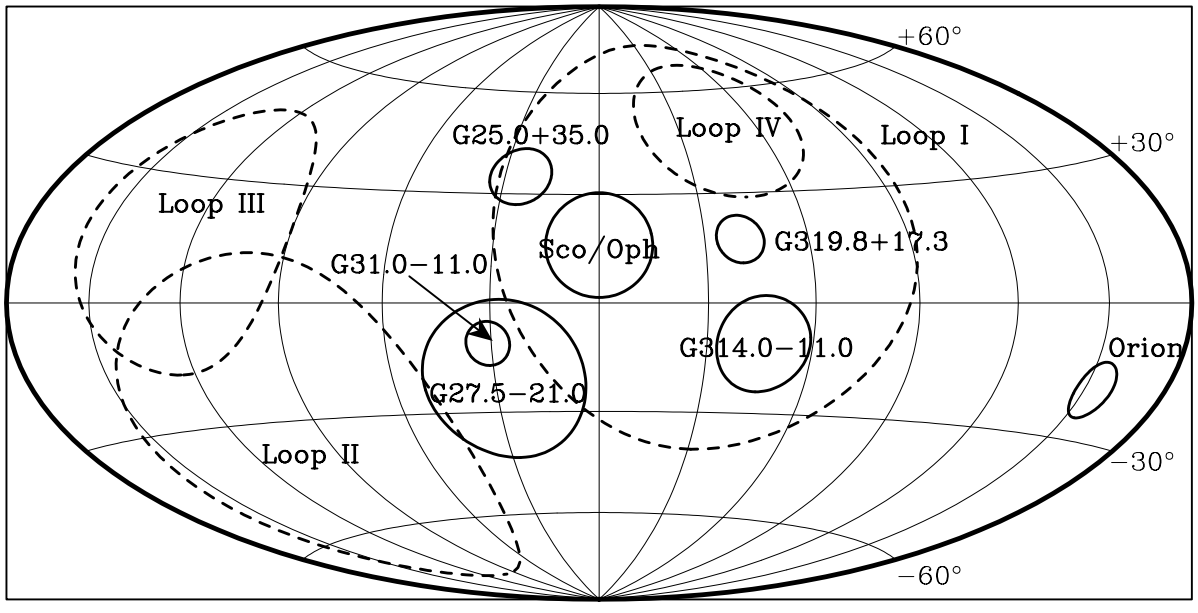

Plate C.1: Original 2326 MHz map.
Total power map of the galactic 2326 MHz emission (extragalactic component subtracted). White contours are drawn at levels of 0.1, 0.2, 0.3 and 0.4 K. Black contours are drawn at levels of 1, 2, 4, 8, 16 and 32 K.

Plate C.2: Diffuse galactic background map (2326 MHz).
See section 6.1 in chapter 6. White contours are drawn at levels of 0.075, 0.1, 0.15, 0.2, 0.25, 0.3, 0.4 and 0.7 K. Black contours are drawn at levels of 1, 2, 4, 8, 16 and 32 K.

Plate C.3: Residual 2326 MHz map.
See chapter 6. White contours are drawn at levels of 0.05, 0.1 and 0.2 K. Black contours are drawn at levels of 0.4, 0.8, 1.6, 3.2 and 6.4 K.

Plate C.4: Residual 408 MHz map.
See chapter 6. White contours are drawn at levels of 5, 10 and 20 K. Black contours are drawn at levels of 40, 80, 160, 320 and 640 K.

Plate C.5: 2326/408 MHz spectral index map.
See section 7.1.2 in chapter 7. Contours are drawn at temperature spectral index (β) levels of 2.1, 2.2, 2.3, 2.4, 2.5, 2.6, 2.7, 2.8 and 2.9.

Plates C.6 to C.14 are maps of the residual thermal and non-thermal emission models for the galactic plane (see section 7.3.2 in chapter 7 and section 8.1 in chapter 8). All of the maps are represented as Cartesian (Plate Carrée) projections of the galactic coordinate system. Previously-catalogued objects in these images are represented by following symbols:

Thermal map (upper image):

- $\times$ HII regions (Sharpless, 1953; Blitz et al., 1982)
- $+$ HII regions (Rodgers et al., 1960a)
- $\cdot$ Recombination lines (Caswell and Haynes, 1987; Lockman, 1989)

Non-thermal map (lower image):

- $\times$ SNRs (Green, 1998)
- $+$ SNRs (Duncan et al., 1997)
- $\oplus$ Pulsars (Taylor et al., 1993)

The dashed and solid circles in the lower maps represent large SNRs, both previously identified (dashed) (Duncan et al., 1997; Green, 1998) and new identifications (solid). Contours are drawn at levels of 1, 2, 4, 8, 16, 32 and 64 Jy.Beam^{-1} in both the upper and lower images.

Plate C.6: Galactic Plane Map ($70° \geq \ell \geq 40°$).

Plate C.7: Galactic Plane Map ($45° \geq \ell \geq 15°$).

Plate C.8: Galactic Plane Map ($20° \geq \ell \geq 350°$).

Plate C.9: Galactic Plane Map ($355° \geq \ell \geq 325°$).

Plate C.10: Galactic Plane Map ($330° \geq \ell \geq 300°$).

Plate C.11: Galactic Plane Map ($305° \geq \ell \geq 275°$).

Plate C.12: Galactic Plane Map ($280° \geq \ell \geq 250°$).

Plate C.13: Galactic Plane Map ($255° \geq \ell \geq 225°$).

Plate C.14: Galactic Plane Map ($230° \geq \ell \geq 200°$).